INTERNATIONAL JOURNAL OF SCIENTIFIC RESEARCH AND INNOVATIVE STUDIES
IJSRIS journal
ISSN: 2820-7157
Advancing Knowledge, Inspiring Innovation
www.ijsrisjournal.com
INDEXED JOURNAL
PEER REVIEWED Rigorous & Transparent | DOI: CROSSREF Member | OPEN ACCESS For Global Visibility | BI-MONTHLY Timely Publication | WIDE READERSHIP High Impact & Visibility | AUTHOR FRIENDLY Fast | Supportive | Reliable

RECEIVED 19 June 2026 | ACCEPTED 10 July 2026 | PUBLISHED 1 August 2026
August 2026 | Volume 5 | Number 4
Pages from: 171 to 188

Rainfall-induced instability of high road cut slopes in tropical lateritic soils: numerical assessment and stabilization performance

Kuele Teneffo Divin-Christ[1], Martial Ngnihamye Nde[1,2], Michel Mbessa[1,3]

[1]Department of Civil Engineering, National Advanced School of Public Works, P.O. Box 510, Yaoundé, Cameroon, kueledivin@gmail.com
[2]Department of Mechanical Engineering, ENSET, University of Douala, P.O. Box 1872, Douala, Cameroon, martialnde@yahoo.fr
[3]Laboratory of Mechanics, Materials, Structures and Production (LMMPS), National Advanced School of Engineering, University of Yaoundé I, P.O. Box 8390

Crossref doi
PREFIX : 10.63883
IJSRIS JOURNAL

ABSTRACT

This study numerically assessed the stability of a high road cut slope subjected to rainfall infiltration, on the Olembe–Obala Interchange Road section near Nkolngem, in the Centre Region of Cameroon. Hourly climatic data spanning 25 years (2000–2025) were obtained from NASA POWER and cross-validated against Climate Research Unit monthly records, yielding a Pearson correlation coefficient of 0.949 and a mean relative error of 9%, confirming data reliability. Extreme rainfall intensities were extracted and fitted to the Gumbel distribution, with adequacy verified by the Kolmogorov-Smirnov test, accepted for 84% of durations analyzed. Intensity-Duration-Frequency curves were then constructed for return periods of 2 to 100 years. Infiltration modeling was performed using SEEP/W, with soil hydraulic properties estimated via the Fredlund and Xing model, under two complementary approaches namely a soil-climate interaction approach using continuous hourly time series, and a unit water flux approach simulating discrete extreme events. Slope stability was evaluated using SLOPE/W, combining the Morgenstern-Price limit equilibrium method and a finite element stress-based approach implemented through SIGMA/W, with both methods yielding consistent results within a mean relative difference of 2.72%. In the absence of stabilization, the safety factor decreased under the combined effect of rainfall intensity and duration, falling below the critical threshold of 1.3 during prolonged events exceeding 24 hours. A multiple linear regression analysis revealed that rainfall duration influences the safety factor approximately eight times more than intensity. Two stabilization techniques were evaluated. Vegetation cover, modeled using the Penman-Monteith evapotranspiration method with parameters representative of tropical grasses, increased the safety factor by 4% to 32% depending on event characteristics, primarily through a gain in superficial cohesion from root reinforcement, and maintained the safety factor above 1.3 even for 24-hour events. Masonry revetments with weep holes reduced the maximum degree of saturation by approximately 20% and raised the safety factor by more than 35% during extreme events, consistently keeping slopes above the required safety threshold. These findings highlight the high sensitivity of unstabilized tropical cut slopes to rainfall infiltration and confirm the effectiveness of both vegetation and masonry revetments as context-adapted stabilization solutions.

Keywords: Rainfall-induced slope failure; Tropical lateritic soils; Transient infiltration; Limit equilibrium method; Finite element method; Slope stabilization.

1. Introduction

Road infrastructure development in sub-Saharan Africa increasingly involves large-scale earthworks in territories characterized by complex topography, steep terrain, and highly weathered tropical soils. In Cameroon, the construction of road cut slopes through lateritic and ferrallitic formations is routine, yet the stability of these structures under intense rainfall remains poorly understood and inadequately addressed in design practice. Recent years have seen a sharp rise in rainfall-induced slope failures with severe consequences. Documented events at Ngouache in 2019, Foumban in 2021, Mimboman and Damas in 2022, Mbankolo in 2023, and Limbe and Bamenda in 2024 resulted in significant loss of life and property damage. Slope failures directly affecting road infrastructure were also recorded at Santchou and Yabassi in 2024. These events share a common trigger: intense or prolonged rainfall episodes. This pattern is consistent with projections from Cameroon's National Observatory on Climate Change, which anticipates an increase in the frequency and magnitude of extreme precipitation events in the coming decades. Against this backdrop, the need for rigorous, quantitative assessment of rainfall-induced slope instability in Cameroon is both scientifically compelling and practically urgent.

Rainfall infiltration destabilizes slopes through two primary mechanisms: the reduction of matric suction in unsaturated soils, which diminishes apparent cohesion, and the buildup of positive pore water pressures, which reduces effective stress and shear strength along potential failure surfaces. These mechanisms are well established in the geotechnical literature. Fredlund and Rahardjo (1993) laid the theoretical foundations for unsaturated soil mechanics, demonstrating that matric suction contributes significantly to the shear strength of partially saturated soils and that its loss under wetting constitutes a primary driver of shallow slope failures. Ng and Menzies (2007) extended this understanding by characterizing the transient hydraulic behavior of unsaturated slopes under rainfall, showing that the rate of saturation propagation depends strongly on soil hydraulic conductivity functions and antecedent moisture conditions. The soil-water characteristic curve and the unsaturated hydraulic conductivity function, as modeled by Gardner (1958) and van Genuchten (1980), have since become standard tools for infiltration analysis in slope stability studies.

Numerical modeling has progressively replaced purely analytical approaches in slope stability assessment, enabling coupled hydromechanical simulations under realistic boundary conditions. The limit equilibrium method (LEM), particularly the Morgenstern-Price formulation which satisfies both force and moment equilibrium, remains widely used for its computational efficiency and transparency (Chowdhury et al., 2010). The finite element method (FEM) offers complementary advantages, resolving the in-situ stress distribution without prescribing a failure surface geometry and capturing nonlinear soil behavior more faithfully (Abramson et al., 2002; Griffiths and Fenton, 2004). Several studies have demonstrated the value of combining both approaches: LEM provides rapid, conservative estimates while FEM yields spatially detailed mechanical responses, and their cross-validation strengthens confidence in stability conclusions. Studies applying this combined framework to tropical lateritic slopes, however, remain scarce, and most available work focuses on either saturated conditions or simplified rainfall scenarios that do not reflect the statistical properties of local extreme events.

The characterization of extreme rainfall through frequency analysis is a prerequisite for realistic infiltration scenarios. The Gumbel extreme value distribution is widely used in hydrology to model annual maximum rainfall intensities, and Intensity-Duration-Frequency (IDF) curves derived from its parameters provide the design rainfall inputs required for slope stability analyses across multiple return periods (Chow et al., 1988). Cameroonian context, however, such analyses are rarely integrated into geotechnical design workflows, and the relative influence of rainfall duration versus intensity on slope stability has received limited quantitative attention. A key finding emerging from the broader literature is that rainfall duration tends to govern cumulative infiltration depth and pore pressure buildup more decisively than peak intensity alone, yet this relationship has not been rigorously quantified for high cut slopes in tropical Central Africa.

Stabilization of road cut slopes in tropical environments typically relies on surface protection, drainage systems, and mechanical reinforcement. Vegetation has been extensively studied as a bio-engineering solution: root networks increase superficial cohesion and evapotranspiration reduces soil moisture, both contributing to improved stability (Wu et al., 1979; Freer, 1991). Rickli and Graf (2009) reported reductions in surface erosion of 60 to 90% and stability gains of up to 55% on vegetated highway slopes after five years, compared to bare surfaces. Masonry revetments with weep holes represent a complementary approach, limiting surface infiltration while allowing excess pore pressure to drain, though their quantitative effect on saturation degree and safety factors under varying rainfall scenarios has been less systematically evaluated.

Despite this body of knowledge, significant gaps persist. First, coupled transient infiltration and slope stability analyses calibrated with locally derived extreme rainfall statistics are largely absent for Cameroonian road infrastructure. Second, the relative contributions of rainfall intensity and duration to safety factor reduction have not been quantified for high cut slopes in tropical lateritic soils. Third, comparative numerical evaluations of vegetation and masonry revetments under identical hydrological loading scenarios, using both LEM and FEM, are not available for this geological and climatic context.

This study addresses these gaps through a numerical investigation of a 10-meter-high road cut slope on the Olembe–Obala Interchange Road section near Nkolngem, Cameroon, constructed in ferrallitic lateritic soil. The specific objectives are: (1) to derive extreme rainfall scenarios from 25 years of hourly climatic data through statistical frequency analysis; (2) to model transient infiltration under both soil-climate interaction and unit water flux approaches using SEEP/W; (3) to quantify the effects of rainfall intensity and duration on pore water pressure distribution, shear strength, and slope safety factor using combined LEM and FEM analyses in SLOPE/W and SIGMA/W; and (4) to evaluate and compare the stabilizing performance of vegetation cover and masonry revetments under identical extreme rainfall scenarios. Section 2 describes the study site and the data collection process. Section 3 presents the methodological framework, from rainfall frequency analysis to infiltration modeling and stability assessment. Section 4 reports and discusses the results, and Section 5 draws conclusions and outlines perspectives for future research.

2. Study site and data

2.1. Site location and geomorphological setting

The study site is located at Nkolngem, a locality in the Centre Region of Cameroon, approximately 18 kilometers north of Yaoundé along national road N04, near the villages of Nkolmbéné and Ekoumdouma. The geographic coordinates of the site are 4°05'52.5"N and 11°32'14.6"E. The slope under investigation is part of the road works for the duplication of the northern penetrating road of Yaoundé (Olembe–Obala Interchange), a 22-kilometer, 2×2 lane infrastructure project co-financed by the Central African States Development Bank (BDEAC) and the Republic of Cameroon.

The site sits on the undulating slopes bordering the central plain surrounding Yaoundé. Local topography is characterized by moderately to steeply inclined hillsides, with elevations generally ranging between 650 and 820 meters above sea level. The landscape consists of a succession of hills and valleys intersected by seasonal watercourses. The study slope itself is a recently excavated, bare cut face presenting a reddish-brown coloration characteristic of the lateritic and ferrallitic soils typical of the South Cameroon Plateau. The slope is 320 meters long, with a maximum vertical height of 10 meters at cross-section pk18+025 and a gradient of 5H:3V (figure 1).

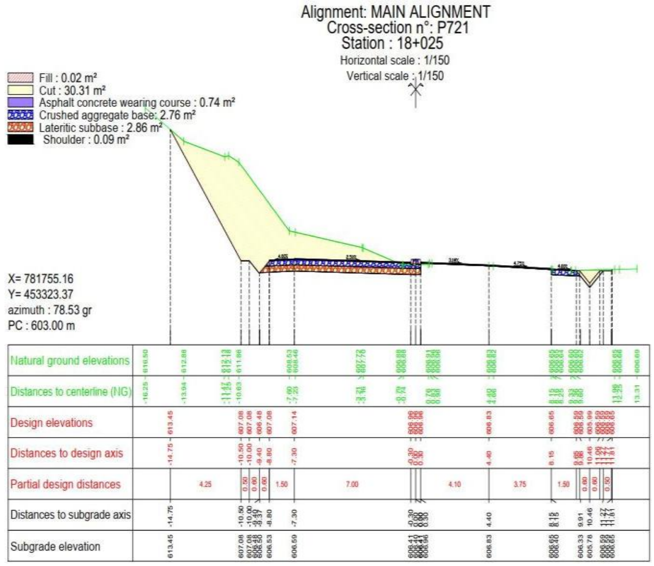

Figure 1. Cross-sectional profile at pk18+025

2.2. Geological and geotechnical characterization

Nkolngem lies within the geological context of the Precambrian basement of the Cameroonian hinterland. The region is dominated by metamorphic and plutonic formations resulting from the Pan-African orogeny (approximately 600 Ma), consisting primarily of gneisses and granites. Surface soils are predominantly ferrallitic, rich in iron and aluminium oxides, with a clayey texture. This ancient basement, extensively weathered at the surface, is locally overlain by a laterite horizon typical of the South Cameroon plateau. The site is drained by a local hydrographic network of small temporary watercourses, generally active during the rainy season, with surface runoff predominating due to the relatively low permeability of lateritic soils.

Geotechnical characterization of the in-situ soil was carried out through unconsolidated undrained (UU) direct shear tests performed according to the LCPC N025 (1987) method. The measured shear strength parameters and physical properties of the soil are summarized in Table 1.

Table 1. Summary geotechnical parameters

γh (t/m³)	Height (mm)	Width (mm)	Ø	γs measured (t/m³)	Approximate soil type	Calibration coefficient (daN/mm)
1.549	20	60	—	2.6176	Lateritic	0.63

Soil specimen characteristics — before testing and shear parameters

No.	γh (t/m³)	γd (t/m³)	w (%)	e	Sr (%)	Vmax	Vcis.
1	1.549	1.238	25.1	1.113	60	1.5	1.2
2	1.553	1.307	18.8	1.001	50	1.5	1.2
3	1.544	1.321	16.9	0.980	46	1.5	1.2
Mean	1.549	1.289	20.3	1.031	52	1.5	1.2

Soil specimen characteristics — after shearing and strength parameters

No.	γ'd (t/m³)	w (%)	σn (bar)	τres (bar)	τpeak (bar)	φp (°)	CUU (bar)	hmax (m)
1	1.238	15.7	0.50	0.612	0.612	21.32	0.53	4.34
2	1.307	17.1	1.00	1.089	1.089	Residual data	—	—
3	1.321	15.4	2.00	1.261	1.261	—	—	—
Mean	1.289	16.053	—	—	—	21.32	0.53	4.34

The elastoplastic Mohr-Coulomb model was selected for this study due to its robustness and suitability for both granular and cohesive soils. This criterion represents the shear failure state of a soil subjected to a given stress level. Its mechanical behavior is governed by the Mohr-Coulomb failure criterion, which expresses the shear strength at failure τ through Equation 1.

$$\tau = c + \sigma \tan(\phi) \quad (1)$$

where c is the soil cohesion, σ is the normal stress, and φ is the internal friction angle. The elastic response prior to yielding is described by the generalized Hooke's law:

$$\boldsymbol{\sigma} = \mathbf{D}\boldsymbol{\varepsilon} \quad (2)$$

where σ is the stress tensor, ε is the strain tensor, and D is the stiffness tensor depending on Young's modulus E and Poisson's ratio ν.

2.3. Climate and hydrology

Hourly climatic data were obtained from the National Aeronautics and Space Administration Prediction Of Worldwide Energy Resources (NASA POWER) database, which provides spatially interpolated surface meteorological parameters at 0.5° × 0.5° spatial resolution. The dataset includes hourly precipitation, air temperature, relative humidity, and wind speed. These data were cross-validated against monthly precipitation records from the Climate Research Unit (CRU) of the University of East Anglia, which aggregates observations from ground-based meteorological stations. Cross-validation was performed by converting NASA POWER hourly data into monthly totals and comparing them with CRU monthly values over the common period, using the mean relative error (MRE) and the Pearson correlation coefficient R, defined respectively by equations 3 and 4.

$$MRE = \frac{1}{n}\sum_{i=1}^{n}\left|\frac{H_i - M_i}{M_i}\right| \times 100 \quad (3)$$

$$R = \frac{\sum(H_i - \bar{H})(M_i - \bar{M})}{\sqrt{\sum(H_i - \bar{H})^2 \sum(M_i - \bar{M})^2}} \quad (4)$$

where H_i and M_i are respectively the monthly totals reconstructed from NASA POWER hourly data and the CRU monthly precipitation values, and $\bar{H}$ and $\bar{M}$ are their respective means.

The site experiences an equatorial Guineo-Congolian climate with two rainy seasons (March–June and September–November) separated by two shorter dry seasons. Mean annual temperature ranges between 24.6°C and 25.6°C, and annual precipitation varies between 1,200 mm and 1,800 mm, with significant interannual variability (Figure 2). Vapor pressure is maintained between 24 and 25.5 hPa, reflecting a persistently humid atmosphere.

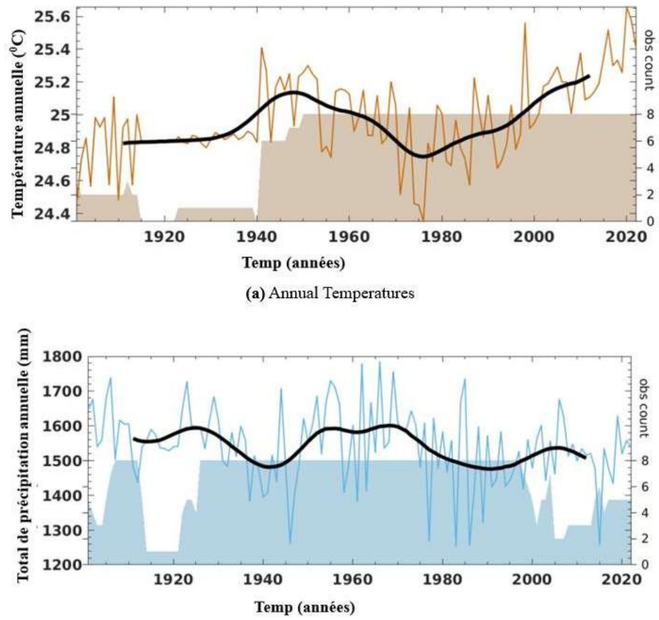

Figure 2. Annual temperatures and total annual precipitation of Nkolngem (Google LLC, 2025)

The temporal distribution of hourly precipitation, air temperature, relative humidity, and wind speed over the study period is illustrated in figure 3, confirming the seasonal pattern described above and the occurrence of episodic high-intensity rainfall events.

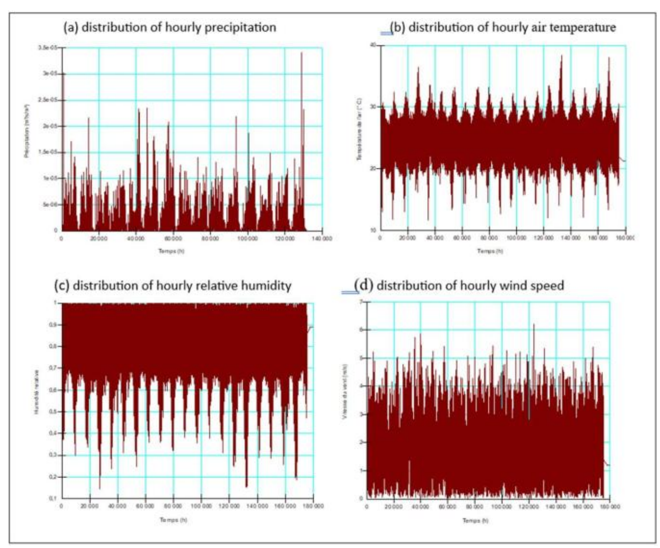

Figure 3. Hourly variations of climatic variables

2.4. Slope geometry and project context

The geometric characteristics of the study slope were extracted from the road project's plan view, longitudinal profile, and cross-sectional drawings. The most critical cross-section, located at chainage pk18+025, defines the reference geometry used for all numerical analyses in this study. As shown in figure 2, the slope has a vertical height of 10 meters and a gradient of 5H:3V.

The numerical model domain extends over a total width of 31.0 meters and a total height of 25.0 meters, with the phreatic surface positioned 18 meters below the top of the model domain. The road surface is treated as an impermeable boundary preventing infiltration, while the slope face and the top surface are exposed to climatic forcing (figure 4).

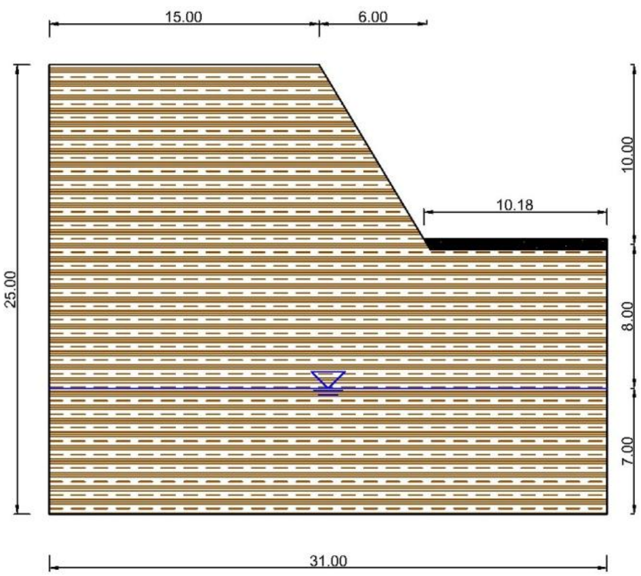

Figure 4. Geometry of the model

3. Methodology

3.1. Rainfall frequency analysis

Extreme rainfall scenarios were derived from the 25-year hourly precipitation record described in Section 2.3 through a three-step procedure: event extraction, statistical fitting, and construction of Intensity-Duration-Frequency (IDF) curves.

Rainfall events were identified from the continuous hourly time series by defining an event as a sequence of consecutive hours with precipitation exceeding a minimum threshold of 1 mm/h, separated from adjacent events by a dry period of at least five hours. For each extracted event, the effective duration was determined, and the average intensity was calculated for each rainfall episode. Subsequently, for each selected duration, the annual maximum intensity series was extracted and used as input for the frequency analysis.

Extreme rainfall intensities were fitted to the Gumbel extreme value distribution, which is widely used in hydrology for modeling annual maximum precipitation (Chow et al., 1988). The cumulative distribution function of the Gumbel distribution is given by formula 6.

$$F(x) = \exp\left[-\exp\left(-\frac{x-\mu}{\beta}\right)\right] \tag{6}$$

The location parameter μ and scale parameter β were estimated by the method of moments as:

$$\mu = \bar{x} - \gamma\beta \tag{7}$$

$$\beta = s\frac{\sqrt{6}}{\pi} \tag{8}$$

where x̄ is the sample mean, s is the standard deviation, and γ = 0.5772 is the Euler-Mascheroni constant. The rainfall intensity corresponding to a return period T was then estimated as:

$$I_T = \mu - \beta\ln\left[-\ln\left(1-\frac{1}{T}\right)\right] \tag{9}$$

The goodness of fit of the Gumbel distribution to the observed data was assessed for each duration using the Kolmogorov-Smirnov (KS) test, a nonparametric test that quantifies the maximum distance between the empirical cumulative distribution function (formula 10) and the theoretical Gumbel cumulative distribution function given by Equation 6.

$$F_e(i) = \frac{i-0.5}{n} \tag{10}$$

where i is the rank of the observation in the ascending-sorted sample and n is the total number of observations. The null hypothesis of Gumbel distribution adequacy was accepted at the 5% significance level when the KS statistic KSD did not exceed the critical value KSC. The results for all 25 durations analyzed are reported in Section 4.1, and the resulting IDF curves for return periods of 2, 5, 10, 20, 50, and 100 years are presented there as well.

3.2. Soil hydraulic property estimation

Two hydraulic property functions are required to model infiltration in partially saturated soil: the soil-water characteristic curve (SWCC), which relates volumetric water content to matric suction, and the unsaturated hydraulic conductivity function, which relates hydraulic conductivity to the degree of saturation or matric suction.

The SWCC was estimated using the equation 11 proposed by Fredlund and Xing (1994), which expresses gravimetric water content W_W as a continuous function of matric suction ψ.

$$W_w = W_s\left[1 - \frac{\ln(1+\psi/h_r)}{\ln(1+10^6/h_r)}\right]\left\{\frac{1}{\ln[e+(\psi/a_f)^{n_f}]}\right\}^{m_f} \tag{11}$$

where W_s is the gravimetric water content at saturation, a_f is a fitting parameter related to the suction at the inflection point, n_f controls the rate of desaturation, m_f describes the curvature at high suction values, h_r is the suction at residual water content, and ψ is the matric suction in kPa. This equation was used in conjunction with the pedotransfer function (PTF) proposed by Fredlund (2000), which estimates the SWCC parameters from the particle-size distribution using the unimodal function:

$$P(d) = \frac{1}{\{\ln[e+(a_{gr}/d)^{n_{gr}}]\}^{m_{gr}}}\left[1 - \left(\frac{\ln(1+d_r/d)}{\ln(1+d_r/d_m)}\right)^7\right] \tag{12}$$

where a_{gr} is a parameter related to the initial break point of the curve, n_{gr} is related to the maximum slope of the curve, m_{gr} describes the shape of the fine portion of the curve, d_r is related to the number of fines in the soil, d is the considered particle diameter, and d_m is the smallest admissible particle diameter.

The fitting parameters n_f and m_f were further estimated through the auxiliary function P(φ):

$$P(\phi) = P_1\left[\frac{1}{\ln\left\{e+\left[\frac{10^{p_4-\log(d_e)}-1}{p_2}\right]^{p_3}\right\}}\right] + p_5 \tag{13}$$

where p_1, p_2, p_3, p_4, and p_5 are curve-fitting parameters, d_e is the effective particle diameter, and P(φ) represents the value of n_f or m_f.

The unsaturated hydraulic conductivity function was estimated using the van Genuchten (1980) model, which expresses the relative hydraulic conductivity K_r as a function of either the relative saturation Θ (Equation 14) or the pressure head h (Equation 15).

$$K_r(\Theta) = \Theta^{1/2}[1-(1-\Theta^{1/m})^m]^2 \tag{14}$$

$$K_r(h) = \frac{\{1-(\alpha h)^{n-1}[1+(\alpha h)^n]^{-m}\}^2}{[1+(\alpha h)^n]^{m/2}} \tag{15}$$

The relative saturation Θ is related to pressure head by:

$$\Theta = [1+(\alpha h)^n]^{-m} \tag{16}$$

where α, n, and $m = 1 - 1/n$ are dimensionless shape parameters and h is the pressure head. The resulting hydraulic property functions for the study soil are presented and discussed in Section 4.2.

3.3. Infiltration modeling framework

Transient infiltration through the slope was modeled using SEEP/W 2024 (GEO-SLOPE International Ltd., 2024), a finite element software specifically designed for the analysis of water flow through porous media under both saturated and unsaturated conditions. SEEP/W solves the two-dimensional governing equation (equation 17) for transient flow.

$$\frac{\partial}{\partial x}\left(k_x\frac{\partial H}{\partial x}\right) + \frac{\partial}{\partial y}\left(k_y\frac{\partial H}{\partial y}\right) + Q = \frac{\partial\theta}{\partial t} \tag{17}$$

where k_x and k_y are the hydraulic conductivities in the horizontal and vertical directions, H is the total hydraulic head, Q is the discharge of a source or sink, θ is the volumetric water content, and t is time.

The model domain, shown in Figure 4, was discretized using predominantly four-node quadrilateral elements with three-node triangular elements in geometrically complex zones. The road surface was assigned an impermeable boundary condition, preventing infiltration through the pavement. From a mechanical point of view, horizontal displacement is restrained along the left and right boundaries, while vertical displacements and rotations remain free. The base of the model is restrained in both horizontal and vertical displacement and remains free in rotation. The initial hydraulic conditions were automatically determined by SEEP/W from the initial phreatic surface position, generating a realistic suction profile throughout the unsaturated zone prior to rainfall application.

Two complementary infiltration modeling approaches were adopted, reflecting the two types of hydrological scenarios considered in this study.

The first approach, referred to as the soil-climate interaction approach, applied a continuous hourly climatic time series directly to the slope surface as a boundary condition. Precipitation, air temperature, relative humidity, and wind speed were prescribed as time-varying inputs over a simulation period of 9,000 days. Under this approach, the actual infiltration flux qI at the soil surface is governed by the water-balance equation:

$$(q_P + q_M)\cos\alpha + q_E + q_R = q_I \quad (18)$$

where q_P is the precipitation flux, q_M is the snowmelt flux (taken as zero in the tropical context of this study), q_E is the evaporation flux, q_R is the runoff flux, and α is the slope angle.

Potential evapotranspiration (PET) was computed using the Penman-Monteith method described by:

$$q_{PET} = \frac{1}{h_{fg}}\left[\frac{\Gamma(q_n - q_g)}{\Gamma + \gamma(1 + r_c/r_a)} + \frac{\rho_a c_p (p_{v0} - p_{va})/r_a}{\Gamma + \gamma(1 + r_c/r_a)}\right] \quad (19)$$

where r_a and r_c are the aerodynamic and canopy resistances, respectively; h_{fg} is the latent heat of vaporization; q_n is the net radiation; q_g is the ground heat flux; ρ_a is the atmospheric air density; c_p is the specific heat capacity of moist air; p_{v0} is the saturated vapor pressure at mean air temperature; p_{va} is the actual vapor pressure at a reference height; Γ is the slope of the saturation vapor-pressure curve; and γ is the psychrometric constant.

$$r_a = \frac{1}{uk^2}\ln\left(\frac{z_{ref} - d}{z_{om}}\right)\ln\left(\frac{z_{ref} - d}{z_{oh}}\right) \quad (20)$$

$$r_c = \frac{r_l}{LAI} \quad (21)$$

where u is the wind speed; k is the von Kármán constant; z_{ref} is the reference height for wind, humidity, and temperature measurements; d is the zero-plane displacement height; z_{om} and z_{oh} are the surface roughness lengths for momentum and heat/vapor fluxes; r_l is the bulk stomatal resistance of a well-illuminated leaf; and LAI is the Leaf Area Index.

The second approach, referred to as the unit water flux approach, applied constant rainfall fluxes corresponding to the design intensities derived from the IDF curves at return periods of 2, 5, 10, 20, 50, and 100 years, for fixed durations of 2 hours and for durations ranging from 1 to 24 hours at a fixed intensity. This approach enabled parametric analysis of the separate effects of rainfall intensity and duration on infiltration response and slope stability.

3.4. Slope stability analysis framework

Slope stability was assessed using SLOPE/W 2024 and SIGMA/W 2024 (GEO-SLOPE International Ltd., 2024), which are fully interoperable with SEEP/W within the GeoStudio 2024 suite, enabling direct transfer of pore water pressure fields computed by SEEP/W into the stability analysis at each time step of the transient simulation. Two complementary analysis methods were employed.

The first is the Morgenstern-Price limit equilibrium method (LEM), which satisfies both force and moment equilibrium and allows for circular, non-circular, or composite failure surfaces, with the interslice force inclination varying according to a user-defined function. The safety factor F from this method is computed iteratively until the force-based safety factor F_f (formula 22) and the moment-based safety factor F_m (formula 23) converge.

$$F_f = \frac{\sum[cl + (N - ul)\tan\phi]\sec\alpha}{\sum[W - (T_{n+1} - T_n)]\tan\alpha + \sum(E_{n+1} - E_n)} \quad (22)$$

$$F_m = \frac{\sum[cl + (N - ul)\tan\phi]}{\sum W\sin\alpha} \quad (23)$$

where c is the soil cohesion; l is the slice-base length; N is the normal force on the slice base; W is the slice self-weight; α is the slice-base inclination; u is the pore-water pressure; φ is the internal friction angle; T_n and T_{n+1} are tangential interslice forces; and E_n and E_{n+1} are horizontal interslice forces.

The second method is the finite element stress-based approach, in which the in-situ stress distribution is first computed by SIGMA/W using the Mohr-Coulomb elastoplastic constitutive model described by Equations 1 and 2. The resulting nodal stresses are then passed to SLOPE/W to compute a stability factor SF:

$$SF = \frac{\sum S_r}{\sum S_m} \quad (24)$$

where the resisting shear force S_r and the mobilized shear force S_m at the base of each column are given by:

$$S_r = \beta_i s = \beta_i[c\prime + (\sigma_n - u_w)\tan\phi\prime] \quad (25)$$

$$S_m = r_m \beta_i \quad (26)$$

where β_i is the column base area, c′ is the effective cohesion, σ_n is the normal stress at the column base, u_w is the pore-water pressure, φ′ is the effective friction angle, and r_m is the mobilized shear stress. The critical safety factor for each scenario was identified by searching a large population of potential failure surfaces for the minimum value.

The combination of LEM and the finite element stress-based approach provide complementary analytical perspectives.

LEM delivers computationally efficient estimates widely recognized in geotechnical engineering practice, while the stress-based finite element approach resolves the spatial distribution of stresses without prescribing a failure surface geometry, offering a more physically complete representation of slope mechanical behavior.

3.5. Stabilization scenarios

Two stabilization techniques were numerically evaluated and compared against the baseline unstabilized condition, namely vegetation cover and masonry revetments with weep holes.

3.5.1. Vegetation cover

Vegetation was modeled within the soil–climate interaction boundary condition of SEEP/W by specifying a set of vegetation parameters representative of tropical grass species, summarized in Table 2.

Table 2. Vegetation parameters

Parameter	Leaf Area Index (LAI)	Plant Moisture Limiting Point	Root Depth	Ground Cover Fraction
Value	1.5	0.2	0.8	75
Unit	m^2/m^2	—	m	%

Vegetation improves slope stability through two mechanisms. First, evapotranspiration driven by the Penman-Monteith formulation (Equation 19) reduces soil moisture and maintains higher matric suction values, thereby preserving a greater proportion of the apparent cohesion contributed by the unsaturated state. Second, the root network provides an additional cohesion increment to the soil, modeled following the formulation of Swanston (1979):

$$c = t_R(\cos\theta \tan\phi + \sin\theta) \tag{27}$$

where t_R is the unit tensile strength of roots, θ is the rotation angle of the failure surface relative to the slope, and φ is the internal friction angle of the soil. This root-cohesion increment was applied as a depth-varying additional cohesion, decreasing from the surface downward in accordance with the reduction in root density with depth, with a root influence depth of 0.8 m.

3.5.2. Masonry revetments with weep holes

Masonry revetments were modeled in SEEP/W as an impermeable barrier covering the slope face, interrupted at regular intervals by weep holes represented as zero total-water-pressure boundary conditions. This configuration allows excess pore water that accumulates behind the revetment to drain freely through the weep holes, preventing the buildup of hydrostatic pressure behind the facing. The geometric configuration of the revetment model, including the positions of the weep holes and the resulting water-flux trajectories, is illustrated in Figure 5.

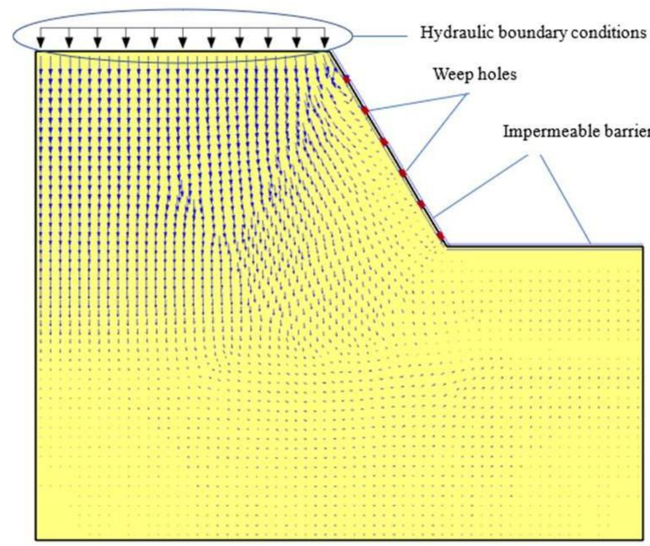

Figure 5. Numerical model of masonry revetment

The stabilizing effect of masonry revetments was modeled to operate primarily through hydraulic means. By limiting surface infiltration, they reduce the degree of saturation within the slope body, thereby restraining pore-pressure development and preserving higher effective-stress levels along potential failure surfaces.

4. Results and Discussion

4.1. Rainfall frequency analysis results

The Gumbel distribution provided a satisfactory fit to the annual maximum intensity series for 21 of the 25 durations analyzed, corresponding to more than 84% of cases, as shown in table 3. The four durations for which the KS test rejected the Gumbel fit at the 5% significance level (2 h, 5 h, 6 h, and 20 h) exhibit slightly elevated empirical variability, likely attributable to the irregular structure of convective rainfall events at these intermediate aggregation scales, which is a known characteristic of equatorial climates (Panthou et al., 2014). Given that the Gumbel distribution was accepted for all surrounding durations and is widely established as appropriate for tropical rainfall frequency analysis, it was retained as a reasonable approximation for these four durations.

Table 3. Kolmogorov-Smirnov test results showing KSD, KSC, and adequacy indicator for each duration from 0.5 h to 24 h

Duration (h)	KSD	KSC	Agreement
0.5	0.311	0.366	1
1	0.232	0.280	1
2	0.200	0.191	0
3	0.147	0.150	1
4	0.257	0.299	1
5	0.149	0.111	0
6	0.145	0.125	0
7	0.094	0.140	1
8	0.118	0.137	1
9	0.077	0.168	1
10	0.065	0.185	1
11	0.085	0.223	1
12	0.168	0.203	1
13	0.088	0.227	1
14	0.086	0.276	1
15	0.135	0.321	1
16	0.107	0.305	1
17	0.227	0.371	1
18	0.139	0.380	1
19	0.139	0.439	1
20	0.513	0.247	0
21	0.187	0.643	1
22	0.365	0.760	1
23	0.206	0.643	1
24	0.145	0.601	1

The resulting IDF curves, presented in figure 6, show that for a given return period, intensity decreases monotonically with increasing duration, reflecting the well-known inverse relationship between rainfall intensity and event duration in tropical convective regimes. For a fixed duration, intensity increases with return period, as expected for extreme value distributions. These IDF curves served as the design rainfall inputs for the unit water flux infiltration scenarios described in Section 3.3.

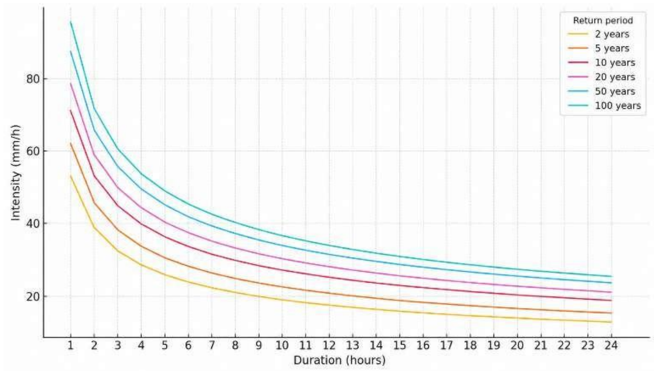

Figure 6. IDF curves

4.2. Soil hydraulic property functions

The estimated soil hydraulic property functions are presented in figure 7. The SWCC shows that volumetric water content remains close to the one at the saturation for matric suctions below approximately 10 kPa, decreases sharply through the transition zone between 10 and 100 kPa, and approaches the residual water content for suctions exceeding 100 kPa. This behavior is characteristic of fine-grained lateritic soils with moderate water retention capacity, consistent with observations reported for similar tropical ferrallitic profiles in Central Africa (Toll et al., 2019). The hydraulic conductivity function remains approximately equal to the saturated conductivity Ks for suctions below 1 kPa and decreases exponentially thereafter, reaching very low values above 100 kPa. This strong suction dependence of hydraulic conductivity is a key driver of the transient infiltration behavior observed in subsequent analyses, as it governs the rate at which the wetting front advances through the slope body under rainfall forcing.

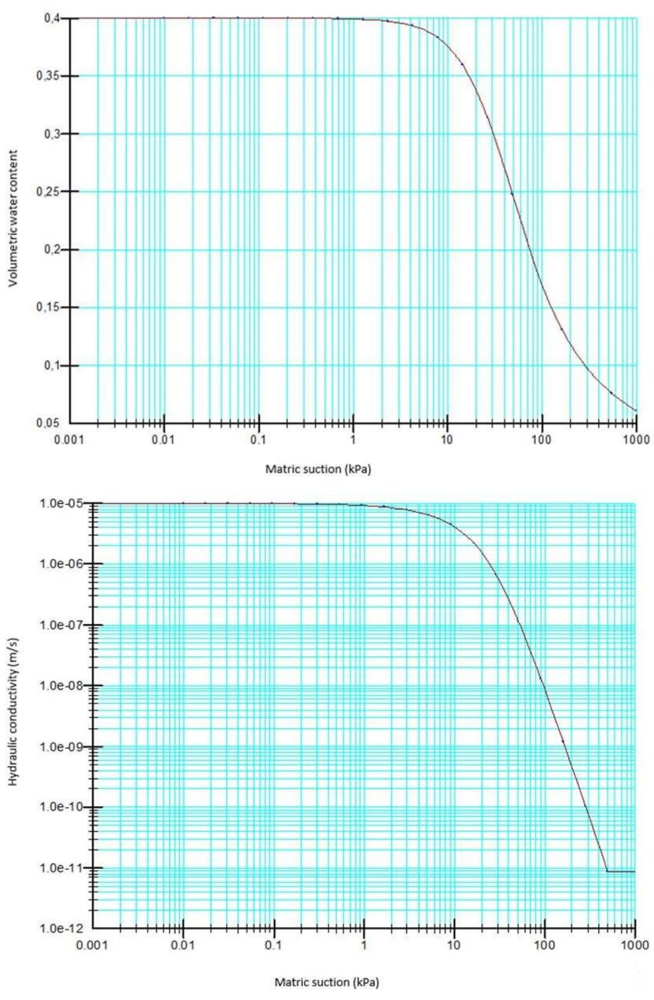

Figure 7. Unsaturated hydraulic conductivity function and SWCC

4.3. Infiltration response under soil-climate interaction

The soil–climate interaction simulation, covering approximately 25 years of continuous climatic forcing, provides a long-term perspective on the hydraulic state of the slope under realistic meteorological conditions. The evolution of pore water pressure behind the slope face over the simulation period is shown in figure 8. The pore water pressure remains predominantly negative throughout the simulation, indicating that the slope operates in an unsaturated state under normal climatic conditions, with matric suction contributing positively to apparent cohesion and slope stability. However, episodic intense rainfall events cause transient inversions of pore water pressure from negative to positive values, temporarily eliminating the suction-related cohesion component and reducing the effective stress along potential failure surfaces. These transient positive pore pressure excursions become progressively more frequent and intense over the simulation period; a trend consistent with the projected increase in extreme precipitation events reported by the National Observatory on Climate Change for the Centre Region of Cameroon. This finding underscores the long-term vulnerability of unstabilized cut slopes in this region under evolving climatic conditions.

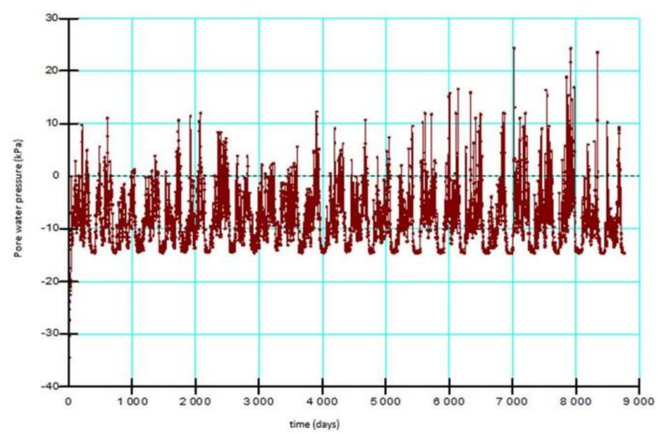

Figure 8. Pore-water pressure over time under soil-climate interaction

4.4. Infiltration response under unit water flux scenarios

4.4.1. Effect of rainfall intensity

The parametric analysis of rainfall intensity effects was conducted by applying the design rainfall intensities corresponding to return periods of 2, 5, 10, 20, 50, and 100 years for a fixed duration of 2 hours. The evolution of pore water pressure and degree of saturation during and after each rainfall event is presented in Figure 9.

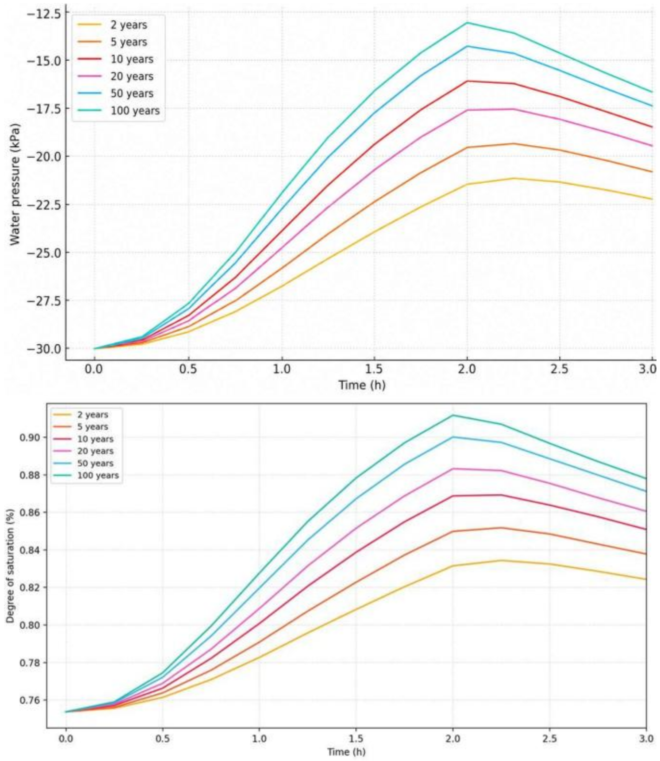

Figure 9. Pore-water pressure and degree-of-saturation evolution over time for return periods of 2 to 100 years at a fixed 2-hour duration

4.4.2. Effect of rainfall duration

The parametric analysis of rainfall duration effects was conducted by applying a fixed design intensity and varying the event duration from 1 to 24 hours. The temporal evolution of the degree of saturation for each duration is presented in figure 10.

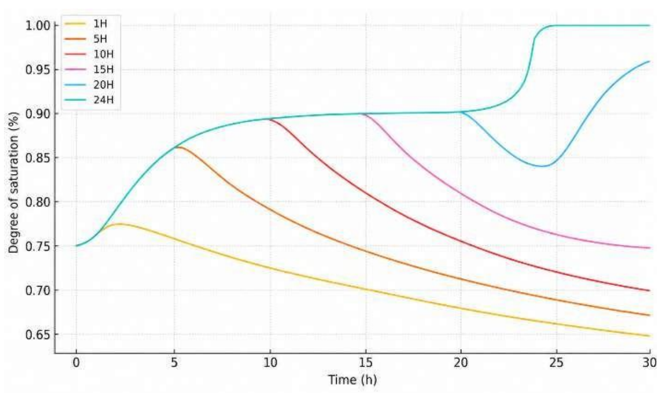

Figure 10. Degree of saturation over time for durations from 1 h to 24 h

Continuously during the rainfall event, reaches a peak at the end of the event, and then decreases progressively as drainage proceeds. For durations exceeding 20 hours, a distinct behavioral transition is observed: after the initial peak at the end of the event, the degree of saturation undergoes a secondary increase several hours later, driven by the continued redistribution of infiltrated water from the surface layers toward deeper horizons. This behavior reflects the progressive saturation of the soil profile under prolonged rainfall, which eventually raises the phreatic surface sufficiently to sustain near-saturated conditions throughout the slope body even after precipitation has ceased. For a duration of 24 hours, no intermediate decrease is observed, and the degree of saturation remains at near-saturated levels throughout, indicating that the slope has reached a state of quasi-complete hydraulic saturation. This duration-dependent behavioral transition has important implications for slope stability, as discussed in Section 4.5.

4.5. Slope stability without stabilization

4.5.1. Effect of rainfall intensity on stability

The evolution of the critical safety factor as a function of return period, computed by both the Morgenstern-Price LEM and the finite element stress-based method, is presented in figure 11. The safety factor in the absence of infiltration, representing the dry initial condition, is also shown as a reference.

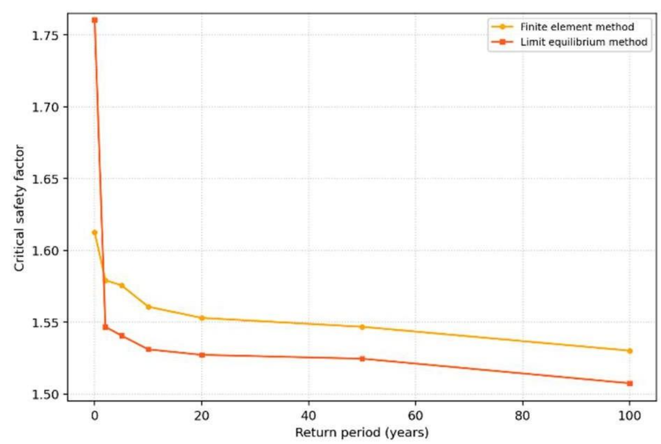

Figure 11. Critical safety factor vs return period for LEM and FEM methods, with dry-condition reference

The safety factor decreases monotonically with increasing return period for both methods, confirming that higher rainfall intensities progressively destabilize the slope through the reduction of matric suction and the buildup of positive pore water pressures. The Morgenstern-Price LEM consistently yields lower safety factor values than the finite element stress-based method across all return periods, confirming its more conservative character, which is consistent with findings reported in the broader slope stability literature (Chowdhury et al., 2010). The finite element stress-based approach, by resolving the actual in-situ stress distribution without prescribing the failure surface geometry, captures a more realistic mechanical response and generally produces higher safety factor estimates. Importantly, both methods yield consistent trends, and their outputs remain in close agreement across all scenarios, with a mean relative difference of 2.72%, providing strong cross-validation of the numerical results.

The shear strength curves as a function of slip distance (figure 12) show a general shape characterized by an initial decrease followed by a progressive increase toward a maximum at depth. This shape reflects the influence of initial stress conditions and the mechanical properties of the soil. Furthermore, a gradual decrease in shear strength is observed with increasing return period, confirming that higher rainfall intensity generally weakens the material and reduces its ability to resist shear stresses.

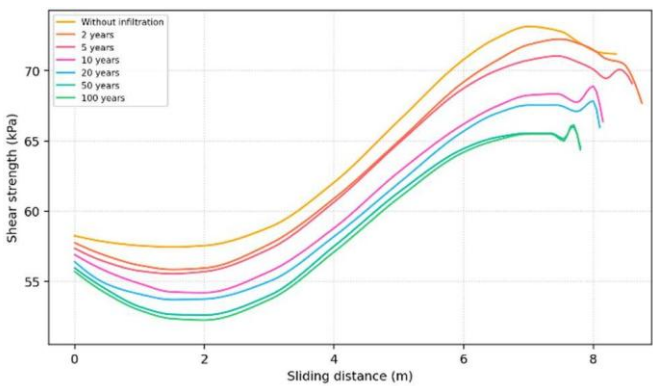

Figure 12. Shear strength as a function of slip distance and return period

4.5.2. Effect of rainfall duration on stability

The evolution of the critical safety factor as a function of rainfall duration for both analysis methods is presented in figure 13. The safety factor decreases progressively with increasing duration, with a pattern that differs qualitatively from the intensity effect described in Section 4.5.1. For short durations (1 to 15 hours), the decrease is relatively gradual. Beyond 15 hours, the rate of safety factor reduction accelerates markedly, consistent with the hydraulic behavioral transition described in Section 4.4.2, in which prolonged infiltration raises the phreatic surface and sustains near-saturated conditions throughout the slope body. At a duration of 24 hours, the safety factor computed by the Morgenstern-Price LEM falls below 1.3, a value commonly cited in practice and in worked examples (Bond et al., 2013) as the indicative minimum for permanent slopes. This indicates that the slope is at risk of failure under prolonged extreme rainfall events even without accounting for the additional destabilizing effect of rising return periods.

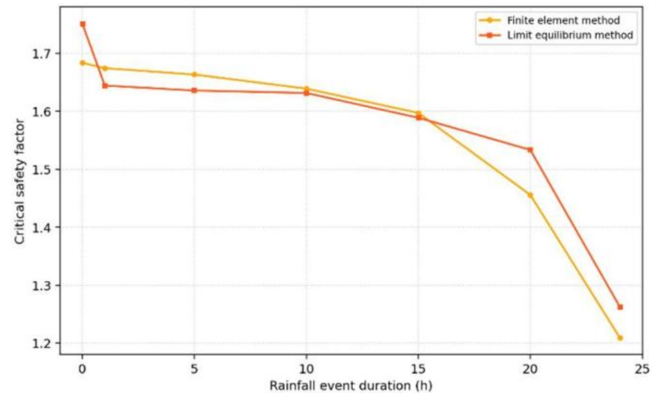

Figure 13. Critical safety factor vs rainfall duration for LEM and FEM methods

The shear strength distribution along the critical failure surface (figure 14), presented as a function of slip distance for each duration, further illustrates this progressive degradation. For durations below 15 hours, shear strength exhibits an initial decrease followed by a recovery at depth, indicating that the deeper soil retains sufficient resistance. For durations exceeding 20 hours, this recovery is no longer observed, and shear strength decreases continuously along the entire failure surface, reflecting a uniformly weakened slope body consistent with near-complete saturation.

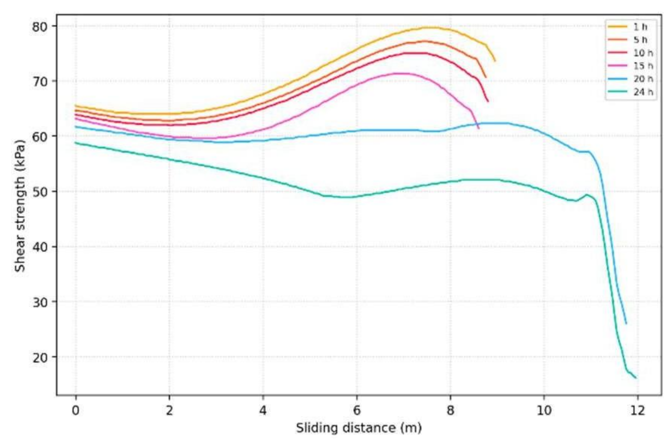

Figure 14. Shear strength as a function of slip distance and rainfall duration

4.5.3. Combined effect of intensity and duration

The combined influence of rainfall intensity and duration on slope stability was quantified through a multiple linear regression analysis of the computed safety factor values. The resulting relationship is given by equation 28.

$$FS = 1.6406 - 0.0014I - 0.011D \tag{28}$$

Where I is the rainfall intensity in mm/h and D is the duration in hours. The coefficient of determination $R^2 = 0.67$ indicates a moderate but statistically meaningful correlation, reflecting the nonlinear nature of the hydromechanical processes underlying slope instability, which a linear model can only partially capture. The regression coefficients reveal that rainfall duration exerts an influence on the safety factor approximately eight times greater in magnitude than rainfall intensity. This finding is physically consistent with the hydraulic behavior described in Sections 4.4.1 and 4.4.2: while intensity governs the rate of surface infiltration and near-surface suction loss, duration controls the cumulative volume of infiltrated water and the depth of phreatic surface rise, which have a far more pervasive effect on the effective stress distribution throughout the slope body.

The safety factor contour map presented in figure 15 provides a comprehensive visualization of this combined effect across the full range of intensity and duration scenarios analyzed.

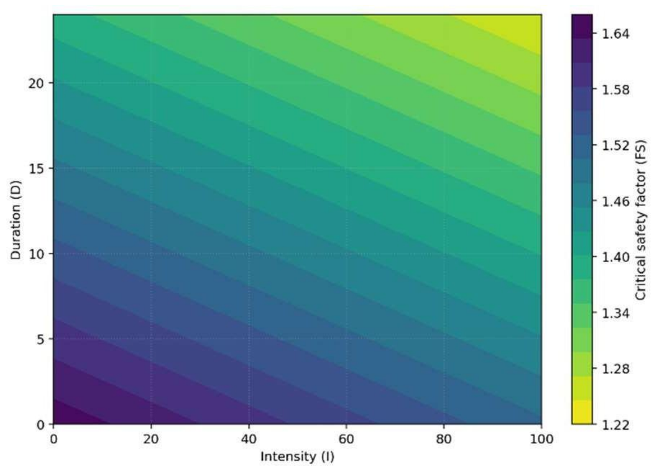

Figure 15. Contour map of safety factor as a function of rainfall intensity and duration

4.6. Effect of stabilization measures

4.6.1. Vegetation cover

The influence of vegetation on slope stability was evaluated under both varying intensity and varying duration scenarios.

Under varying intensity conditions, the pore water pressure evolution shows systematically lower values for the vegetated slope compared to the bare slope across all return periods, reflecting the combined effect of evapotranspiration-driven moisture reduction and the maintenance of higher matric suction. This difference diminishes for return periods exceeding 50 years, where the rainfall flux overwhelms the evapotranspiration capacity of the grass cover, causing the hydraulic responses of the vegetated and bare slopes to converge (figure 16).

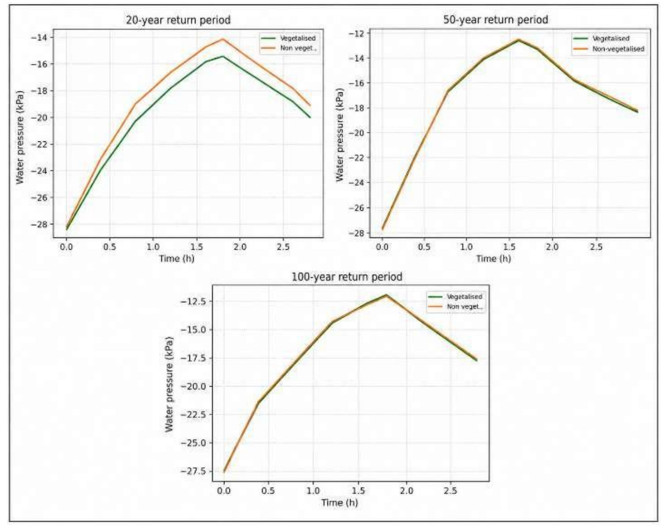

Figure 16. Evolution of water pressure over time for selected return periods, with and without vegetation

Under varying duration conditions, the safety factor comparison presented in figure 17 reveals that vegetation maintains the safety factor above the threshold of 1.3 even for the critical 24-hour event that causes failure of the unstabilized slope. This result confirms the effectiveness of vegetation as a stabilization measure for high road cut slopes in tropical lateritic soils under the rainfall regime characteristic of the Cameroon Centre Region.

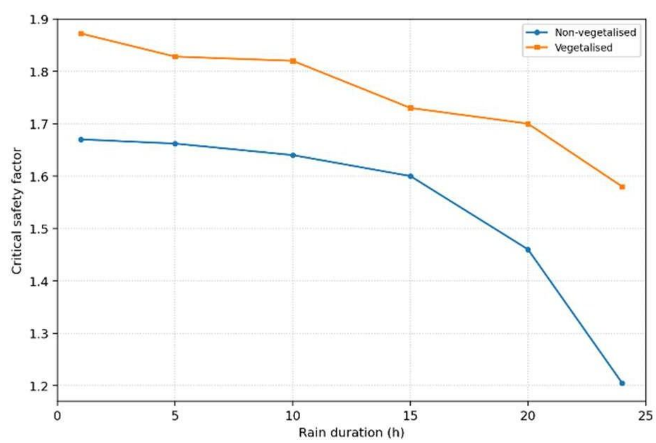

Figure 17. Safety factor vs rainfall duration with and without vegetation

Of Rickli and Graf (2009), who highlighted the significant stabilizing effect of vegetation on shallow slopes and landslide-prone areas, and with the work of Cammeraat et al. (2005), who demonstrated that root density, architecture, and reinforcement depth strongly influence vegetation-induced slope stabilization.

4.6.2. Masonry revetments with weep holes

The influence of masonry revetments on slope stability was similarly evaluated under both intensity and duration scenarios. The degree of saturation evolution presented in figure 18 shows that the revetment reduces the maximum degree of saturation within the slope body by approximately 20% relative to the unprotected case across all return periods analyzed. This reduction is achieved by intercepting surface infiltration and redirecting water through the weep holes, thereby limiting the volume of water entering the slope body and preventing the progressive phreatic surface rise that drives pore pressure buildup.

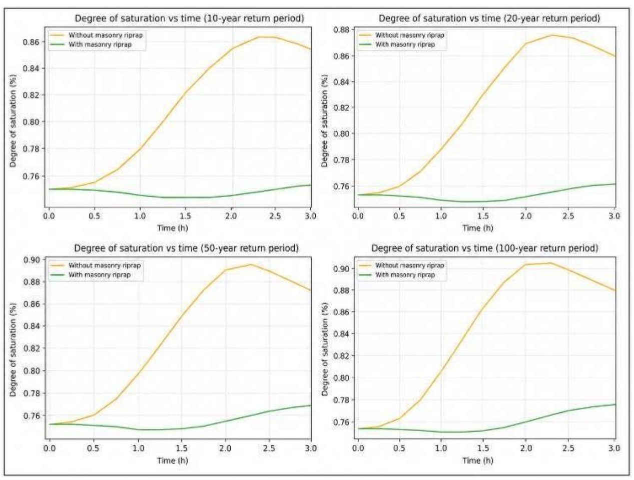

Figure 18. Degree of saturation over time with and without masonry revetments for varying return periods

Under varying duration conditions, the degree of saturation is significantly reduced by the presence of the revetment, with the effect becoming more pronounced as duration increases. The revetment prevents the near-complete saturation observed in the unprotected case for events exceeding 20 hours, maintaining the degree of saturation at stable or decreasing levels even after the end of the rainfall event. The safety factor improvement under varying duration conditions, shown in figure 19, confirms that masonry revetments maintain the slope above the critical threshold even for the 24-hour extreme event, with a safety factor increase exceeding 35% relative to the unstabilized baseline.

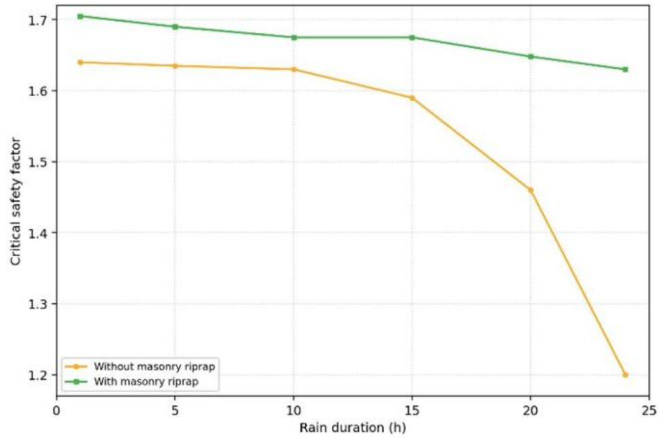

Figure 19. Safety factor vs rainfall duration with and without masonry revetments

4.7. Discussion

The results presented in Sections 4.3 to 4.6 collectively demonstrate that rainfall-induced slope instability in high road cut slopes on the Olembe–Obala road section is governed primarily by the duration of rainfall events, with duration having approximately eight times greater influence on safety factor reduction. This finding extends and quantifies a trend that has been qualitatively noted in several studies on tropical slope stability. Rahardjo et al. (2008) observed that prolonged moderate rainfall events were more consistently associated with slope failures in Singapore than short intense storms, attributing this to the greater cumulative infiltration depth achieved over time. Mukhlisin et al. (2011) reached similar conclusions for volcanic slopes in Malaysia, where the phreatic surface response to rainfall was found to be more sensitive to event duration than to peak intensity. The present study provides a quantitative regression-based partitioning of intensity and duration effects for a high lateritic cut slope in Central Africa, supported by a combined LEM and finite element analysis framework validated against 25 years of climatic data.

The behavioral transition observed at approximately 15 to 20 hours of continuous rainfall, beyond which safety factor reduction accelerates markedly, corresponds physically to the point at which the infiltration front reaches the phreatic surface and begins raising it within the slope body. This threshold behavior has important implications for the design of early warning systems. A cumulative rainfall duration threshold of approximately 15 hours at moderate to high intensity could serve as a practical alert criterion for slope monitoring on this road section, complementing conventional intensity-based thresholds.

The two stabilization techniques evaluated exhibit distinct and complementary mechanisms. Vegetation acts through a combination of hydraulic moderation via evapotranspiration and mechanical reinforcement via root cohesion, providing consistent improvements across the full range of rainfall scenarios. Its effectiveness diminishes under extreme events because the evapotranspiration capacity of the grass cover is overwhelmed by high infiltration fluxes, limiting the hydraulic benefit to the mechanical root cohesion component alone. Masonry revetments, by contrast, act primarily through direct hydraulic interception of surface infiltration, producing larger absolute improvements in safety factor but requiring more substantial investment in construction and maintenance. The choice between these two techniques, or their combination, should therefore be guided by the specific rainfall regime, the available budget, and the acceptable level of residual risk.

5. Conclusion

This study has provided a framework for quantitative understanding of rainfall-induced instability in high road cut slopes constructed in tropical lateritic soils, through a coupled transient infiltration and slope stability analysis framework calibrated against 25 years of climatic data and applied to a representative case study on the Olembe–Obala road section in Cameroon.

The most significant finding is that rainfall duration governs slope stability reduction approximately eight times more strongly than rainfall intensity for the slope and soil conditions investigated. This relationship, quantified through multiple linear regression analysis across a systematic matrix of intensity and duration scenarios, departs from the intensity-focused thresholds that dominate current geotechnical practice in Cameroon and much of sub-Saharan Africa. The physical basis lies in the nonlinear hydraulic response of the partially saturated lateritic soil: while intensity controls the rate of surface infiltration and near-surface suction loss, duration determines the cumulative infiltration volume and the extent of phreatic surface rise, which exerts a far more pervasive influence on effective stress distribution throughout the slope body. The identification of a behavioral transition at approximately 15 to 20 hours of continuous rainfall, beyond which safety factor reduction accelerates markedly, offers a physically grounded basis for the calibration of early warning thresholds on instrumented slopes in similar geological and climatic settings.

The cross-validation of the Morgenstern-Price limit equilibrium method and the finite element stress-based approach, with a mean relative difference of 2.72% across all scenarios, confirms that these methodologically distinct frameworks produce consistent stability assessments for transient infiltration conditions, reinforcing confidence in the numerical results and supporting the use of the computationally efficient limit equilibrium approach for practical design applications in this context.

Vegetation and masonry revetments address slope instability through fundamentally different mechanisms. Vegetation provides consistent safety factor improvements of 4% to 32% and maintains the slope above the threshold of 1.3 even under the critical 24-hour event that causes failure of the unstabilized slope, though its hydraulic benefit diminishes under very high intensity events. Masonry revetments reduce the maximum degree of saturation by approximately 20% and increase the safety factor by more than 35% under extreme events, providing a larger margin of safety. These quantitative differences suggest that masonry revetments should be prioritized in areas with a significant probability of exposure to extreme rainfall events, particularly in situations where the acceptable level of risk is low, while vegetation offers a cost-effective and environmentally beneficial solution for moderate scenarios and as a complementary measure in hybrid stabilization systems.

Beyond this case study, the methodological framework developed here is transferable to other high cut slopes across tropical Central Africa, where deeply weathered lateritic profiles, high rainfall variability, and projected intensification of extreme precipitation events create a growing infrastructure risk that current empirical design practices are not yet well equipped to address. Future research should extend this framework toward probabilistic analysis incorporating spatial variability of soil properties, adopt more advanced constitutive models capable of representing progressive structural degradation of lateritic soils under repeated wetting and drying cycles, and evaluate hybrid stabilization systems to support the development of context-adapted design guidelines for tropical road infrastructure.

- **Credit authorship contribution statement**

Kuele Teneffo Divin-Christ: Writing – original draft, Writing – review & editing, Visualization, Validation, Methodology, Investigation, Formal analysis, Data curation, Conceptualization. Michel Mbessa: Writing – review & editing, Supervision, Validation, Methodology, Conceptualization, Project administration. Nde Ngnihamye Martial: Writing – review & editing, Supervision, Validation, Methodology, Visualization, Conceptualization.

- **Declaration of competing interest**

The authors declare that they have no known competing financial interests or personal relationships that could have appeared to influence the work reported in this paper.

- **Acknowledgement**

The authors gratefully acknowledge the Ministry of Public Works of Cameroon, as the project owner of the case study, and INTEGC as construction supervision mission, for providing the geometric, geotechnical, and project data essential to this study. The authors also thank the National Advanced School of Public Works of Yaoundé for institutional support. The climatic data used in this study were obtained from the NASA Prediction of Worldwide Energy Resources (NASA POWER) database, provided by the NASA Langley Research Center, and from the Climate Research Unit (CRU) of the University of East Anglia.

- **Data availability**

The data presented in this study are available upon request from the corresponding authors.

References

1. Abramson L. W., Lee T. S., Sharma S., Boyce G. M. (2002). Slope stability and stabilization methods. John Wiley & Sons, 2e éd., Hoboken (New Jersey). 736 p. ISBN 978-0-471-38493-9.

2. Adje Kpie J. D. T., Anoosheh I. (2021). Mechanism and techniques of measuring of suction. International Journal for Modern Trends in Science and Technology. pp.99–104. https://doi.org/10.46501/IJMTST0707017

3. Cammeraat, E., van Beek, R., Kooijman, A., (2005). Vegetation succession and its consequences for slope stability in SE Spain. Plant and Soil, 278, 135–147. https://doi.org/10.1007/s11104-0055893-1

4. Beakawi H. M., Baghabra O. S. (2018). A review on the angle of repose of granular materials. Powder Technology, vol.7. pp. 397417. https://doi.org/10.1016/j.powtec.2018.02.003

5. Budhu M. (2011). Soil mechanics and foundations. John Wiley & Sons, Hoboken (États-Unis). 784 p. ISBN 978-1-118-13604-1.

6. CEMAGREF (1997). Techniques de stabilisation des talus – Guide méthodologique. CEMAGREF, Rotterdam (Pays-Bas). 124 p.

7. Chowdhury R., Flentje P., Bhattacharya G. (2010). Geotechnical Slope Analysis. CRC Press (Taylor & Francis Group), London (Royaume-Uni). 788 p. ISBN 978-0-415-46974-6. https://doi.org/10.1201/9780203864203

8. Das B. M., Sobhan K. (2018). Principles of geotechnical engineering. Cengage Learning, 9e éd., Boston (États-Unis). 704 p. ISBN 978-1-305-97093-9.

9. Espinosa Fuentes S. A., El Naggar M. H. (2025). Uncertainty Analysis and Quantification of Rainfall-Induced Slope Instability in Fine-Grained Clayey Soils. Geotechnics, vol.5. pp. 31. https://doi.org/10.3390/geotechnics5020031

10. Fredlund D. G., Xing A. (1994). Equations for the soil-water characteristic curve. Canadian Geotechnical Journal, vol.31.pp. 521–532. https://doi.org/10.1139/T94-061

11. GEO-SLOPE International Ltd., (2024). Stability Modeling with SLOPE/W: An Engineering Methodology. GEO-SLOPE International Ltd., Calgary, Canada.

12. Ghobadian R., Afzalimehr H., Riahi-Madvar H. (2013). Hydraulic performance of masonry lining in steep canals. Journal of Civil Engineering and Urbanism, vol.3. pp. 209-213.

13. Griffiths D. V., Fenton G. A. (2004). Probabilistic slope stability analysis by finite elements. Journal of Geotechnical and Geoenvironmental Engineering, vol.130. pp. 507-518. https://doi.org/10.1061/(ASCE)1090-0241(2004)130:5(507)

14. IDRRIM (Institut des Routes, des Rues et des Infrastructures pour la Mobilité) (2024). Guide des terrassements des remblais et des couches de forme : Fascicule 1-Principes généraux. Cerema, collection Références, Bron (France). 120p. ISBN 978-2-37180-678-8.

15. Johnston I., Murphy W., Holden J. (2024). The effects of internal erosion on granular soils used in transport embankments. Soils and Foundations, vol.64. pp. 101-424. https://doi.org/10.1016/j.soildyn.2024.101424

16. Karstunen M., Amavasai A. (2017). BEST SOIL: Soft soil modelling and parameter determination. Chalmers University of Technology, Department of Architecture and Civil Engineering, Gothenburg (Suède). 84p. ISBN 978-91-984301-0-3.

17. Knappett J. A., Craig R. F. (2012). Craig's Soil Mechanics. CRC Press, 8e éd, London (Royaume-Uni). 584 p. ISBN 978-0-415-56125-9.

18. LCPC, Ministère de l'Écologie (2010). Prévention et stabilisation des glissements de terrain : Conception, mise en œuvre et maintenance des dispositifs. Laboratoire Central des Ponts et Chaussées – Collection Techniques et méthodes des laboratoires des Ponts et Chaussées, Paris (France). 161 p. ISBN 978-2-7208-2585-9.

19. Magnan J.-P., Mestat P. (1997). Lois de comportement et modélisation des sols. Techniques de l'Ingénieur, vol.218. pp. 1–23. https://doi.org/10.51257/a-v1-c218

20. Magnan J.-P., Meyer G. (2018). Influence des interactions entre écrans de soutènement sur le calcul de la butée. Revue Française de Géotechnique, n° 154, pp.2. http://dx.doi.org/10.1051/geotech/2018002

21. NASA POWER Project. (2025). NASA Prediction of Worldwide Energy Resources (POWER) Data Access Viewer. NASA Langley Research Center. Retrieved from https://power.larc.nasa.gov/

22. Ng, C.W.W., Menzies, B., (2007). Advanced Unsaturated Soil Mechanics and Engineering. Taylor & Francis, London, United Kingdom. 687 p.

23. Rahardjo H., Hritzuk K. J., Leong E. C., Rezaur R. B. (2003). Effectiveness of horizontal drains for slope stability. Engineering Geology, vol.69. pp. 295–308. https://doi.org/10.1016/S0013-7952(02)00288-0

24. Rahardjo, H., Nio, A.S., Leong, E.C., Song, N.Y., (2008). Effects of groundwater table position and soil properties on stability of slope during rainfall. Journal of Geotechnical and Geoenvironmental Engineering, 136, 1555–1564. https://doi.org/10.1061/(ASCE)GT.1943-5606.0000385

25. Rickli C., Graf F. (2009). Effects of forests on shallow landslides – case studies in Switzerland. Forest, Snow and Landscape Research, vol.82. pp. 33–44. https://www.dora.lib4ri.ch/wsl/islandora/object/wsl:15351

26. Riheb H. (2020). Introduction à la mécanique des sols. Université Ferhat Abbas de Sétif 1, Sétif (Algérie). 150 p.

27. Sangeeta S., Maheshwari B. K. (2016). Slope Stability Evaluation by Different Limit Equilibrium Methods. INDOROCK-Journal.pp. 23.

28. Shiferaw H. M. (2021). Study on the influence of slope height and angle on the factor of safety and shape of failure of slopes based on strength reduction method of analysis. Beni-Suef University Journal of Basic and Applied Sciences, vol 10. pp. 1–17. https://doi.org/10.1186/s43088-021-00115-w

29. Wu T. H., McKinnell W. P., Swanston D. N. (1979). Strength of tree roots and landslides on Prince of Wales Island, Alaska. Canadian Geotechnical Journal, vol.16. pp. 19–33. https://doi.org/10.1139/T79-003

30. Xie X., Wang L. (2023). A Review on Soil Suction and its Determination Methods. Journal of Innovation and Development, vol.3. pp.102-104. https://doi.org/10.54097/jid.v3i2.9394